Analysis of an asymmetric resonant cavity as a beam monitor

David H. Whittum[a)]
Stanford Linear Accelerator Center, Stanford University, Stanford, California 94309

Yury Kolomensky
California Institute of Technology, Pasadena, California 91125

We analyze the excitation of an arbitrary, externally coupled resonant structure by a charged particle beam, providing a rigorous formulation of the effect of spurious modes and intrinsic mode nonlinearity on inferred beam coordinates. Results are illustrated for a two-cavity system employed for beam-position monitoring with an idealized front-end signal processor. © *1999 American Institute of Physics.* [S0034-6748(99)01403-3]

I. INTRODUCTION

Charged particle beams are powerful tools with which to dissect the fundamental laws of nature and today high energy physicists sift through the rubble of beam collisions searching for deviations in the predictions of the Standard Model at the level of 1 part per million. High precision studies of this kind require exquisite control of the beams, and this implies a requirement to *monitor* the relevant attributes of the particle distribution. One such beam monitor consists of a resonant cavity. Historically, these have been employed to monitor beam phase and position, and their precision has not been particularly stressed—the original resonant cavity beam position monitors employed at Stanford circa 1965, were required to function with a resolution at the level of ±1 mm.[1] However, modern applications require resolution at the level of ±1 μm or smaller.[2]

In this work, we analyze a resonant cavity as a pickup, to discern the essential systematic effects that appear in such devices when high precision is required. One of the specific problems that motivated this work is a resonant beam-position monitor (BPM) cavity to be used for a fixed-target experiment (''E158'') at Stanford.[3] This experiment requires precise beam-position monitoring to permit accurate inference of beam-angle on-target. *A priori* one is inclined to design and build special-purpose cavities for this purpose. However, for reasons of cost, it is of interest to make use of existing cavities—rectangular cavities with a single coaxial output. For such cavities, and at the 1 μm level in beam-position monitoring, the effect of nonlinear field components on the inferred beam position must be quantified. Moreover, one would like to know if it would be useful to retrofit such cavities, and how one might do this, to improve the precision.

Beyond the application to this specific BPM system, experimental studies in other resonant structures suggest the need for a thorough analysis of the problem. For example, conventional accelerating structures possess dipole modes and these have been instrumented to detect beam position.[4,5] In addition, in recent years, interest has developed in miniature *planar* accelerating structures.[6,7] Unlike the conventional axially symmetric accelerating structures, the planar structures produce a fundamental accelerating mode containing a quadrupolar component. This focusing or defocusing component is a serious issue for beam dynamics. Analysis presented here provides the framework for characterization of such structures as pickups or kickers.

In Sec. II, we set down the theory of a resonant cavity pickup, providing a simple formulation categorizing the multipole coefficients required to describe field nonlinearities in an asymmetric electromagnetic resonator, including differential external coupling. We compute mode excitation by a tri-Gaussian bunch, and, using superposition, we determine the excitation by a train of such bunches. In Sec. III we illustrate these considerations for the case of the beam position monitor system proposed for E158. This includes analysis of the mode characteristics of the two cavity geometries proposed, supplemented with bench measurements. In Sec. IV, adopting an idealized model for the front-end signal processor, we go on to illustrate and quantify the effect of parasitic modes, and nonlinearities. This discussion and the bench measurements provide a rigorous starting point for the E158 BPM error analysis. In Sec. IV, we offer some conclusions.

II. THEORY OF A RESONANT CAVITY PICKUP

In this section, we analyze Maxwell's equations for a cavity with waveguide coupling, wall losses, and beam excitation, reducing it to a simple circuit equivalent. We then quantify excitation of this circuit by a single tri-Gaussian bunch, and a train of such bunches.

A. Equivalent circuit

We consider first an idealized, lossless cavity with no external coupling. In the approximation of isolated, nondegenerate resonances, and considering frequencies below cutoff in the beam port, we express the solution for the cavity electric field as a superposition of modes,

$$\mathbf{E}(\mathbf{r},t) = \sum_\lambda \mathbf{E}_\lambda(\mathbf{r}) e_\lambda(t),$$

a)Electronic mail: whittum@slac.stanford.edu

with mode index λ, and the convention that modal fields $\mathbf{E}_\lambda(\mathbf{r})$ are normalized to unit volume integral. The excitation of mode amplitude e_λ by current density $\mathbf{J}$ may be expressed in terms of the overlap integral, evaluated in the frequency domain

$$\tilde{J}_\lambda = \int d^3\mathbf{r}\,\tilde{\mathbf{J}}\cdot\mathbf{E}_\lambda,$$

where Fourier components are denoted by an overtilde. The response of a cavity mode is then given by

$$(\omega^2 - \omega_\lambda^2)\tilde{e}_\lambda = j\omega\frac{1}{\epsilon_0}\tilde{J}_\lambda,$$

with ϵ_0 the electrical permittivity of free space, $1/\epsilon_0 = cZ_0$, with $Z_0 \approx 376.7\,\Omega$, and c the speed of light. The angular frequency is ω, and ω_λ is the mode resonance. To incorporate external coupling in our model, it is convenient to amend our choice of unperturbed modal basis to refer to the solution of the Helmholtz equation, with *open-circuit* boundary conditions on a reference plane located in the connecting guide. Since the waveguide modes form a complete set we may expand the electric field on this reference plane, and quantify the coupling in terms of the overlap integral $V_{1\lambda}$ on the plane, of the modal electric field, and the fundamental mode of the connecting guide.[8] In this way we arrive at the external Q,

$$\frac{1}{Q_{e\lambda}} = \frac{V_{1\lambda}^2}{\epsilon_0\omega_\lambda Z_{c1}},$$

where Z_{c1} is the characteristic impedance of the waveguide mode. Explicitly, $Z_{c1} = Z_0(\omega/c\beta)$ for a TE mode, and $Z_{c1} = Z_0$ for a TEM mode. In terms of external Q, our mode equation is revised to read

$$(\omega^2 - \omega_\lambda^2)\tilde{e}_\lambda = j\omega\frac{1}{\epsilon_0}\tilde{J}_\lambda - \frac{j\omega\omega_\lambda}{Q_{e\lambda}}\frac{(\tilde{V}_1^+ - \tilde{V}_1^-)}{V_{1\lambda}},$$

and continuity of tangential electric field at the port-plane requires $\tilde{V}_1^+ + \tilde{V}_1^- = \tilde{e}_\lambda \tilde{V}_{1\lambda}$. The quantities $\tilde{V}_1^+$, $\tilde{V}_1^-$ are the incoming and outgoing voltage phasors at the plane, referred to the impedance Z_{c1}. Thus incident and outgoing power in steady state are $P^\pm = |\tilde{V}_1^\pm|^2/2Z_{c1}$, and the net power flowing into the cavity is $P^+ - P^-$. For a cavity excited only by beam, with output looking into a matched load, $P^+ = 0$.

Incorporating wall losses, and redefining the mode resonance frequency to incoporate the shift due to the reactive part of the wall impedance, we augment this result to read

$$(\omega^2 - \omega_\lambda^2)\tilde{e}_\lambda = j\omega\frac{1}{\epsilon}\tilde{J}_\lambda - \frac{j\omega\omega_\lambda}{Q_{e\lambda}}\frac{(\tilde{V}_1^+ - \tilde{V}_1^-)}{V_{1\lambda}} + j\frac{\omega\omega_\lambda}{Q_w}\tilde{e}_\lambda,$$

with Q_w the wall Q.

To make this more explicit, we consider a ballistic pencil beam, with current density

$$\mathbf{J} = \hat{z}\delta^2(\mathbf{r}_\perp - \mathbf{r}_{\perp b})I_b\!\left(t - \frac{z}{V}\right), \tag{1}$$

where I_b is the beam current waveform, t is the time coordinate, z is the coordinate displacement down the beamline, $\mathbf{r}_\perp$ is the coordinate in the transverse plane, and δ is the delta

TABLE I. First few multipoles, column (2) takes the coefficient b_n, and column (3), a_n.

Term	n	Normal	Skew
Monopole	0	1	$\cdots$
Dipole	1	x	$-y$
Quadrupole	2	$x^2 - y^2$	$-2xy$
Sextupole	3	$x^3 - 3xy^2$	$y^3 - 3x^2y$
Octupole	4	$x^4 - 6x^2y^2 + y^4$	$4xy(y^2 - x^2)$
Decapole	5	$x^5 - 10x^3y^2 + 5xy^4$	$10x^2y^3 - y^5 - 5x^4y$

function. The beam is assumed to be ballistic, traveling at speed V in the z-direction, centered on the transverse coordinate $\mathbf{r}_{\perp b}$. The Fourier transform is

$$\tilde{\mathbf{J}}(\mathbf{r},\omega) = \hat{z}\delta^2(\mathbf{r}_\perp)\int_{-\infty}^{\infty}\frac{d\omega}{\sqrt{2\pi}}e^{-j\omega t}I_b\!\left(t - \frac{z}{V}\right)$$

$$= \hat{z}\delta^2(\mathbf{r}_\perp - \mathbf{r}_{\perp b})\tilde{I}_b(\omega)e^{-j\omega z/V},$$

and we assume no variation of beam centroid along the beam. The overlap integral $\tilde{J}_\lambda = \tilde{I}_b(\omega)\tilde{w}_\lambda^*(\mathbf{r}_{\perp b})$, where

$$\tilde{w}_\lambda(\mathbf{r}_{\perp b}) = \int_{-\infty}^{+\infty}dz\,E_{z\lambda}(\mathbf{r}_\perp = \mathbf{r}_{\perp b},z)e^{j\omega z/V}; \tag{2}$$

we will see that this quantity is central to the analysis of the coupling of the beam to the cavity. We observe that

$$\nabla_\perp^2\tilde{w}_\lambda = \int_{-\infty}^{+\infty}dz\,e^{j\omega z/V}\nabla_\perp^2 E_{z\lambda}(\mathbf{r}_\perp,z)$$

$$= \int_{-\infty}^{+\infty}dz\,e^{j\omega z/V}\!\left(-\frac{\partial^2}{\partial z^2} - \frac{\omega_0^2}{c^2}\right)E_{z\lambda}(\mathbf{r}_\perp,z)$$

$$= \left(\frac{\omega_0^2}{V^2} - \frac{\omega_0^2}{c^2}\right)\int_{-\infty}^{+\infty}dz\,e^{j\omega z/V}E_{z\lambda}(\mathbf{r}_\perp,z)$$

$$= \left(\frac{\omega_0^2}{V^2} - \frac{\omega_0^2}{c^2}\right)\tilde{w}_\lambda,$$

and conclude that for a highly relativistic beam $\tilde{w}_\lambda$ is a *harmonic* function,

$$\nabla_\perp^2\tilde{w}_\lambda = 0, \tag{3}$$

and therefore may be expanded in multipoles,

$$\tilde{w} = \sum_{m=0}^{\infty}r^m[b_m\cos(m\phi) - a_m\sin(m\phi)], \tag{4}$$

where we introduce cylindrical coordinates $(x,y) = r(\cos\phi,\sin\phi)$, and complex multipole coefficients b_m, a_m. The possible leading-order behaviors near the beam-axis are seen in Table I.

Thus far, we have reduced Maxwell's equations to a single relation,

$$(\omega^2 - \omega_\lambda^2)\tilde{e}_\lambda = j\omega\frac{1}{\epsilon_0}\tilde{I}_b(\omega)\tilde{w}_\lambda^*(\mathbf{r}_{\perp b}) - \frac{j\omega\omega_\lambda}{Q_{e\lambda}}\frac{(\tilde{V}_1^+ - \tilde{V}_1^-)}{V_{1\lambda}}$$

$$+ j\frac{\omega\omega_\lambda}{Q_w}\tilde{e}_\lambda; \tag{5}$$

however, with the mode classification, we may cast this in a more transparent form, making clear the essential circuit parameters. To do this we must make a choice of reference impedance, and there exists a convention for this, at least in the case of a pure monopole mode, the convention being to refer to cavity excitation in terms of the voltage *witnessed by the beam*. The voltage drop experienced by a test particle traveling at speed V in the z direction at offset $\mathbf{r}_\perp$, and passing $z=0$ at time $t=t_0$ is

$$V_c(\mathbf{r}_\perp,t_0)=\int_{-\infty}^{+\infty}dz E_z\left(\mathbf{r}_\perp,z,t_0+\frac{z}{V}\right). \tag{6}$$

We may express this in terms of the modal decomposition,

$$E_z\left(\mathbf{r}_\perp,z,t_0+\frac{z}{V}\right)=\sum_\lambda \mathbf{E}_{z\lambda}(\mathbf{r}_\perp,z)e_\lambda\left(t_0+\frac{z}{V}\right),$$

corresponding to which we have

$$V_c(\mathbf{r}_\perp,t_0)=\sum_\lambda V_{c\lambda}(\mathbf{r}_\perp,t_0),$$

where, in the frequency domain,

$$\widetilde{V}_{c\lambda}(\mathbf{r}_\perp,\omega)=\int_{-\infty}^\infty \frac{d\omega}{\sqrt{2\pi}}e^{-j\omega t_0}\widetilde{V}_{c\lambda}(\mathbf{r}_\perp,t_0)=\widetilde{e}_\lambda\widetilde{w}_\lambda(\mathbf{r}_\perp) \tag{7}$$

and our mode equation may be re-expressed in terms of the more meaningful normalizations, $\widetilde{V}_c$, $\widetilde{I}_b$, according to

$$\left(\omega^2-j\frac{\omega\omega_\lambda}{Q_{w\lambda}}-\omega_\lambda^2\right)\widetilde{V}_{c\lambda}(\mathbf{r}_\perp,\omega)$$
$$=-\frac{j\omega\omega_\lambda}{Q_{e\lambda}}n(\widetilde{V}_1^+-\widetilde{V}_1^-)+2j\omega K_{\lambda,\mathbf{r}_\perp,\mathbf{r}_{\perp b}}\widetilde{I}_b, \tag{8}$$

with

$$K_{\lambda,\mathbf{r}_\perp,\mathbf{r}_{\perp b}}=\frac{1}{2\epsilon_0}\widetilde{w}_\lambda^*(\mathbf{r}_{\perp b})\widetilde{w}_\lambda(\mathbf{r}_\perp), \tag{9}$$

$$n_\lambda=\frac{\widetilde{w}_\lambda(\mathbf{r}_\perp)}{V_{1\lambda}}. \tag{10}$$

The continuity condition is most naturally expressed in terms of the transformed forward voltage in the connecting guide $V_{F\lambda}=n_\lambda\widetilde{V}_1^+$, and reverse voltage $V_{R\lambda}=n_\lambda\widetilde{V}_1^-$, as $V_{c\lambda}=V_{F\lambda}+V_{R\lambda}$. It will be convenient to refer to

$$\left[\frac{R}{Q}\right]_{\lambda,\mathbf{r}_\perp}=\frac{4K_\lambda(\mathbf{r}_\perp)}{\omega_\lambda}=\frac{4K_{\lambda,r_\perp,r_\perp}}{\omega_\lambda}, \tag{11}$$

in terms of which the turns ratio is given by

$$|n_\lambda|^2=\frac{2Q_{e\lambda}K_\lambda(\mathbf{r}_\perp)}{Z_{c1}}=\frac{Q_{e\lambda}[R/Q]_{\lambda,\mathbf{r}_\perp}}{2Z_{c1}}, \tag{12}$$

the stored energy

$$U_\lambda=\frac{1}{2}\epsilon_0|\widetilde{e}_\lambda|^2=\frac{|\widetilde{V}_{c\lambda}|^2}{4K_\lambda(\mathbf{r}_\perp)}=\frac{|\widetilde{V}_{c\lambda}|^2}{\omega_\lambda[R/Q]_{\lambda,\mathbf{r}_\perp}}, \tag{13}$$

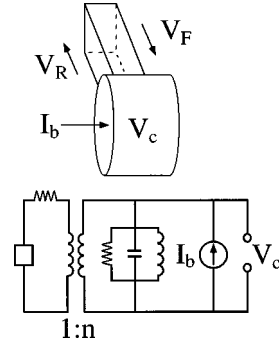and the net power flowing into the cavity

FIG. 1. Sketch of the dynamic variables for a single cavity mode coupled to a waveguide fundamental mode, and a beam. Also shown is an equivalent circuit for the cavity-beam-waveguide system with output waveguide terminated in a matched load. No ''beam-loading'' admittance appears in parallel with the beam current, insofar as we have made the approximation of a highly relativistic beam.

$$P_w=\frac{|\widetilde{V}_{F\lambda}|^2-|\widetilde{V}_{R\lambda}|^2}{2n_\lambda^2 Z_{c1}}$$
$$=\frac{|\widetilde{V}_{F\lambda}|^2-|\widetilde{V}_{R\lambda}|^2}{4Q_{e\lambda}K_\lambda(\mathbf{r}_\perp)}=\frac{|\widetilde{V}_{F\lambda}|^2-|\widetilde{V}_{R\lambda}|^2}{Q_{e\lambda}[R/Q]_{\lambda,\mathbf{r}_\perp}}. \tag{14}$$

In the time domain, our result may be expressed most simply as

$$\left(\frac{d^2}{dt^2}+\frac{\omega_\lambda}{Q_{L\lambda}}\frac{d}{dt}+\omega_\lambda^2\right)V_{c\lambda}=2\frac{\omega_\lambda}{Q_{e\lambda}}\frac{dV_{F\lambda}}{dt}-2K_\lambda(\mathbf{r}_{\perp b})\frac{dI_b}{dt}, \tag{15}$$

and we have introduced the port-loaded Q,

$$\frac{1}{Q_{L\lambda}}=\frac{1}{Q_{w\lambda}}+\frac{1}{Q_{e\lambda}}. \tag{16}$$

This formulation comes with the picture of Fig. 1. It is convenient in that it reduces the problem to an uncomplicated RLC circuit, with an ideal current generator, and an external coupling through a transformer with turns ratio n_λ. However, it contains within it a choice of reference axis, $\mathbf{r}_\perp$, affecting the definition of the cavity voltage, the turns ratio, and the loss factor. This might seem awkward; in fact, it is essential to understanding the operation of the circuit as a monitor of beam coordinates. With the work of this section, we have reduced our system to that of a simple circuit as described by Eq. (15), and depicted in Fig. 1.

B. Characterization of modes

The generalized loss factor, K_λ, is a useful figure of merit to gauge the magnitude of the coupling of the beam to the cavity mode. For example, for a point bunch of charge Q_b, one can show that prior to evanescence the induced voltage is $V_{c\lambda}(t)=-2K_\lambda Q_b\cos(\omega_\lambda t)H(t)$, with H the step function. Work done by the charge at offset $\mathbf{r}_\perp$ on the cavity mode is then $U_\lambda=-\int dt V_{c\lambda}(\mathbf{r}_\perp,t)I_b(t)=K_\lambda Q_b^2$. In addition to the *longitudinal* kick provided by the cavity voltage in mode λ, $V_{c\lambda}(t)$, the cavity may also provide a *transverse* kick, determined from

$$\mathbf{P}_\perp(\mathbf{r}_\perp,t) = \int_{-\infty}^{+\infty} dz \left\{ \frac{1}{V}\mathbf{E}_\perp + \hat{z}\times\mathbf{B}_\perp \right\}_{(\mathbf{r}_\perp,z,t+z/V)}.$$

One can show that

$$\frac{\partial \boldsymbol{P}_\perp}{\partial t} = -\boldsymbol{\nabla}_\perp V, \tag{17}$$

as first noted by Panofsky and Wenzel.[9] In the frequency domain, we may express the kick as

$$\widetilde{\mathbf{P}}_\perp = \frac{j}{\omega}\sum_\lambda \widetilde{e}_\lambda \boldsymbol{\nabla}_\perp \widetilde{w}_\lambda. \tag{18}$$

Thus $\widetilde{w}_\lambda$ determines the form of both the longitudinal and transverse kicks.

Evidently, we may examine and categorize modes of a cavity, based on the harmonic properties of $\widetilde{w}_\lambda$. In practice, this is assessed by examination of $[R/Q]_{\lambda,\mathbf{r}_\perp}$, as computed with an electromagnetic field solver. In general, a mode may contain any or all harmonic components; however, symmetries will delimit the actual terms present. For example, for a cavity respecting cylindrical symmetry, the multipole sum of Eq. (4) reduces to a single azimuthal harmonic, m. The symmetric mode, with $m=0$, must then have $\widetilde{w}_\lambda$ independent of the transverse coordinate. Thus the waveform output by such a mode will be independent of beam position. This result contrasts with the Bessel function dependence of the closed-cavity mode; cancellations occur due to fringe fields near the cavity entrance and exit.

For other than circular cavities, the constraints one may place on the mode character are limited by the number of symmetries present. For example, in a cavity with a reflection symmetry, we may delineate modes based on whether $\widetilde{w}_\lambda$ is even or odd with respect to reflection. For a cavity with *mid-plane* symmetry (symmetric upon $y \rightarrow -y$), we may expect to find modes odd ("skew") in y, and modes even ("normal") in y. Thus a predominantly monopole mode for such a cavity is described by $\widetilde{w} = b_0 + b_1 x + b_2(x^2-y^2)$ $+\cdots$. The coupling parameter b_0 may be quantified more colloquially by the $[R/Q]$ evaluated on-axis,

$$\lim_{\mathbf{r}_\perp \to 0}\left[\frac{R}{Q}\right] = 2\frac{|\widetilde{w}_\lambda(\mathbf{r}_\perp=0)|^2}{\epsilon_0\omega_\lambda} = \frac{2Z_0 c}{\omega_\lambda}|b_0|^2. \tag{19}$$

In light of our analysis, we understand that this conventional parameterization in terms of $[R/Q]$ is *incomplete*. Additional phenomena lurk in the higher components. In terms of $B_n = b_n/b_0$, we may write the accelerating voltage as

$$V_c(x,y,t_0) = \mathcal{R}V_0 e^{j\psi_0}\{1 + B_1 x + B_2(x^2-y^2) + \cdots\},$$

where $V_0 e^{j\psi_0} \equiv \widetilde{V}(\mathbf{r}_\perp=0,t_0)e^{j\omega t_0}$, i.e., V_0 is the maximum accelerating voltage, and ψ_0 the phase, witnessed on-axis. Evidently, an off-axis trajectory corresponds to a different amplitude and phase. Keeping only the dipole correction, and expressing $B_1 = |B_1|e^{\psi_1}$, one can see that

$$V_c(x,y,t_0) \approx \mathcal{R}V_0 e^{j\psi_0}e^{j\delta\psi}(1 + 2|B_1|x\cos\psi_1 + |B_1|^2 x^2)^{1/2},$$

where

$$\tan\delta\psi = \frac{|B_1|x\sin\psi_1}{1 + |B_1|x\cos\psi_1}.$$

Thus the absence of a reflection symmetry permits a phase and an amplitude *asymmetry* in the accelerating voltage. This is generally undesirable in an accelerating cavity, as discussed at some length in Ref. 1. Conversely, such a cavity would not be an ideal phase monitor. An additional consequence is the presence of transverse deflections associated with this mode,

$$\boldsymbol{P}_c = \boldsymbol{\nabla}_\perp \mathcal{R}V_0 e^{j\psi_0}\frac{j}{\omega}[1 + B_1 x + B_2(x^2-y^2) + \cdots],$$

or, at lowest order

$$P_x \approx -\frac{1}{\omega}V_0|B_1|\sin(\psi_0 + \psi_1).$$

Thus particles phased on crest ($\sin\psi_0=0$) experience a transverse deflection determined by the imaginary part of B_1, the phase asymmetry of the mode. Thus, not surprisingly, such an asymmetric geometry provides acceleration *at an angle*, given by $\alpha \approx -|B_1|c\psi_1/\omega$ for small asymmetry, and particles phased on crest.

For the remainder of this work, we will be considering a cavity reflecting a higher degree of symmetry, reflection symmetry in both x and y. We label modes according to their lowest order behavior, and proceed to characterize their higher-order features. For monopole modes, we have at lowest order residual normal quadrupole and octupole components,

$$\widetilde{w}_{\text{even-even}} = b_0[1 + B_2(x^2-y^2) + B_4(x^4-6x^2y^2+y^4)$$
$$+ O(r_\perp^6)\cdots]. \tag{20}$$

For vertical dipole modes, we have residual skew sextupole and skew decapole components,

$$\widetilde{w}_{\text{even-odd}} = -a_1 y[1 + A_3(3x^2-y^2) + A_5(y^4+5x^4-10x^2y^2)$$
$$+ O(r_\perp^6)\cdots], \tag{21}$$

where $A_n = a_n/a_1$, and the coupling parameter a_1 may be quantified in terms of

$$\left[\frac{R_\perp}{Q}\right] = \lim_{\mathbf{r}_\perp \to 0}\frac{1}{y^2}\left[\frac{R}{Q}\right] = \frac{2Z_0 c}{\omega_\lambda}|a_1|^2 \quad (y \text{ dipole}). \tag{22}$$

Similarly, horizontal dipole modes may contain a residual normal sextupole and normal decapole component

$$\widetilde{w}_{\text{odd-even}} = b_1 x[1 + B_3(x^2-3y^2) + B_5(x^4-10x^2y^2+5y^4)$$
$$+ O(r_\perp^6)\cdots]. \tag{23}$$

We have at lowest order,

$$\left[\frac{R_\perp}{Q}\right] = \lim_{\mathbf{r}_\perp \to 0}\frac{1}{x^2}\left[\frac{R}{Q}\right] = \frac{2Z_0 c}{\omega_\lambda}|b_1|^2 \quad (x \text{ dipole}). \tag{24}$$

One can go a step farther with this, and ask, of the modes allowed by symmetry, which are present? Does a cavity have a normal quad mode? When the cavity beam ports respect the symmetry of the cavity proper, one may infer the
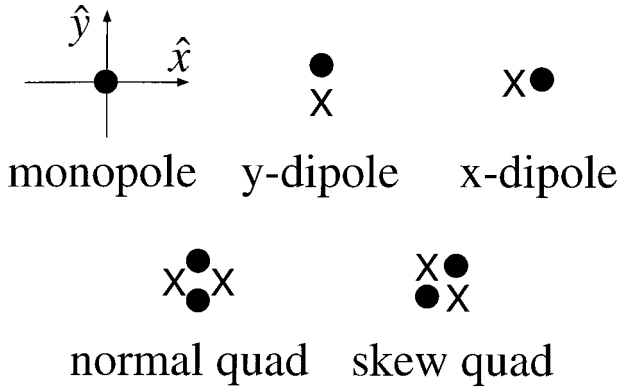
FIG. 2. Integrated longitudinal electric field (synchronous integral) configuration for various modes of a generic cavity respecting x and y inversion symmetries, viewed end-on, from the beam direction.

form of the kick function from the symmetry of the corresponding mode of the unperturbed (closed) cavity. In this way, one may map TM modes of the closed cavity to the ''TM-like'' modes of the cavity with beam ports. To enumerate all modes, however, one must consider as well the TE modes of the closed cavity, for with the addition of beamports, these modes will develop longitudinal fringe electric fields that can couple to the beam. Consequently, a real cavity driven by a beam will exhibit a richer mode spectrum than one would expect from a closed-pillbox analysis. For a qualitative illustration, consider a cavity of rough dimensions $a \times d \times b$. We suppose the x-dimension a is larger than the y-dimension d. To construct the modes, we match actual electric field lines to the integrated field pattern as depicted in Fig. 2. Characteristic wave numbers are of order $\beta_x \approx \pi/a$, $\beta_y \approx \pi/d$, and $\beta_z \approx \pi/b$. One expects a monopole mode derived from the lowest TM mode of the cavity, with frequency $f \approx c\beta_0/2\pi$, where $\beta_0^2 \approx \beta_x^2 + \beta_y^2$. Next one expects to find two dipole modes, an x dipole with $\beta_0^2 \approx (2\beta_x)^2 + \beta_y^2$, and a y dipole at $\beta_0^2 \approx \beta_x^2 + (2\beta_y)^2$. The next modes would be TE-derived dipole modes (or hybrid modes), corresponding to $\beta_0^2 \approx \beta_x^2 + \beta_z^2$ (y dipole, hybrid) and $\beta_0^2 \approx \beta_y^2 + \beta_z^2$ (x dipole, hybrid). Clearly, where the modes actually fall in frequency depends on b. For large b, the hybrid dipole modes come first, for very short b, they are preceded by still other modes. A specific illustration of these considerations for an existing cavity follows in Sec. III.

Finally, let us make the cavity formulation explicit for the case of monopole and dipole modes. To isolate clearly the dependence on beam position, it will be convenient to employ Eq. (15) in the form

$$\left(\frac{d^2}{dt^2} + \frac{\omega_\lambda}{Q_{L\lambda}} \frac{d}{dt} + \omega_\lambda^2 \right) V_{c\lambda}$$

$$\approx 2 \frac{\omega_\lambda}{Q_{e\lambda}} \frac{dV_{F\lambda}}{dt} - 2 k_\lambda \frac{d}{dt} X_\lambda(\mathbf{r}_{\perp b}) I_b(t), \qquad (25)$$

where $X_\lambda = w_\lambda^*(\mathbf{r}_{\perp b})/w_\lambda^*(\mathbf{r}_{\perp 0})$, $k_\lambda = K_{\lambda, \mathbf{r}_{\perp 0}, \mathbf{r}_{\perp 0}}$, and we will take the limit $\mathbf{r}_{\perp 0} \to 0$ for the reference integration path, and augment our convention for mode normalization such that $w_\lambda(\mathbf{r}_{\perp 0})$ is real. For a predominantly monopole mode,

$$X_\lambda(x,y) = 1 + B_{2\lambda}^*(x^2 - y^2) + B_{4\lambda}^*(x^4 - 6x^2y^2 + y^4)$$

$$+ O(\langle r_\perp^6 \rangle) \cdots \qquad (26)$$

and

$$|n_\lambda| = \left(\frac{Q_{e\lambda} \left[\frac{R}{Q} \right]_\lambda}{2Z_c} \right)^{1/2} = \left(\frac{R_\lambda}{2Z_c\beta_\lambda} \right)^{1/2}, \qquad (27)$$

where $\beta_\lambda = Q_{w\lambda}/Q_{e\lambda}$ and the unloaded shunt impedance is $R_\lambda = Q_{w\lambda}[R/Q]_\lambda$ (another convention employs half this value). Power flowing out of the cavity is $-P_w$, where

$$P_w = \frac{|V_{F\lambda}|^2 - |V_{R\lambda}|^2}{2Z_c|n_\lambda|^2} = \beta_\lambda \frac{|V_{F\lambda}|^2 - |V_{R\lambda}|^2}{R_\lambda}. \qquad (28)$$

For a predominantly dipole mode, an x-dipole mode for definiteness, we select an integration path at $x = x_0$, and take the limit $x_0 \to 0$, so that our description of the cavity is resolved in terms of the on-axis voltage gradient,

$$V_{c\lambda}' = \lim_{x_0 \to 0} \frac{V_{c\lambda}}{x_0} \equiv \frac{\partial V_{c\lambda}}{\partial x}$$

and we obtain

$$\left\{ \frac{d^2}{dt^2} + \frac{\omega_\lambda}{Q_{L\lambda}} \frac{d}{dt} + \omega_\lambda^2 \right\} V_{c\lambda}'$$

$$= 2 \frac{\omega_\lambda}{Q_{e\lambda}} \frac{dV_{F\lambda}'}{dt} - 2 k_{\perp\lambda} \frac{d}{dt} X_{b\lambda}(\mathbf{r}_{\perp b}) I_b, \qquad (29)$$

where $k_{\perp\lambda} = \omega_\lambda[R_\perp/Q]_\lambda/4$, and $X_{b\lambda}(\mathbf{r}_{\perp b}) = \lim_{x_0 \to 0} x_0 \times X_\lambda(\mathbf{r}\perp b)$, or

$$X_{b\lambda}(x,y) = x + B_{3\lambda}^*(x^3 - 3xy^2) + B_{5\lambda}^*(x^5 - 10x^3y^2 + 5xy^4)$$

$$+ O(\langle r_\perp^7 \rangle) \cdots . \qquad (30)$$

The continuity condition takes the form $V_{c\lambda}' = V_{F\lambda}' + V_{R\lambda}'$, and the conversion to waveguide impedance is $V_{F\lambda}' = n_\lambda' V_1^+$, $V_{R\lambda}' = n_\lambda' V_1^-$. Stored energy is

$$U_{c\lambda} = \frac{|V_{c\lambda}'|^2}{\omega_\lambda[R_\perp/Q]_\lambda}, \qquad (31)$$

and energy conservation determines that

$$|n_\lambda'| = \left(\frac{Q_{e\lambda} \left[\frac{R_\perp}{Q} \right]_\lambda}{2Z_c} \right)^{1/2} = \left(\frac{R_{\perp\lambda}}{2Z_c\beta_\lambda} \right)^{1/2}, \qquad (32)$$

where the unloaded transverse shunt impedance is $R_{\perp\lambda} = Q_{w\lambda}[R_\perp/Q]_\lambda$. Net power flowing out of the cavity and up the waveguide is $-P_w$, where

$$P_w = \frac{|V_{F\lambda}'|^2 - |V_{R\lambda}'|^2}{2Z_c n_\lambda'^2} = \beta_\lambda \frac{|V_{F\lambda}'|^2 - |V_{R\lambda}'|^2}{R_{\perp\lambda}}. \qquad (33)$$

Where one cavity is coupling several modes, it is helpful to be able to transform to a common impedance. So for example, where one cavity is functioning with both a dipole and a monopole mode, one would appreciate a prescription for adding induced voltages on the connecting waveguide. This is straightforward given the relation of the quantities V_R and V_R' to the waveguide voltage coefficient V_1^- normalized

with respect to the waveguide mode characteristic impedance Z_c. Thus we expect the contribution due to a monopole mode to take the form $V_1^- = V_R/n$ and that due to a dipole mode $V_1^- = V_R'/n'$. In general, it need not be the case that the reference plane for both of these modes is the same, and thus there may be a relative phase between the two mode contributions. If we refer both voltages to the normalization employed for dipole mode quantities, the monopole cavity voltage must be multiplied by a phase factor, and $n'' = n'/n$, or

$$|n''| = \left(\frac{Q_{ed}[R_\perp/Q]_d}{Q_{em}[R/Q]_m} \right)^{1/2}. \qquad (34)$$

With the analysis of this section in-hand, we are in a position to determine the cavity emitted signal, V_1^- due to interaction of any particular mode with a beam, and to superimpose the voltage from the ''design'' or ''desired'' mode with other, parasitic modes, to quantify the effect on resolution. We turn next to apply this model to a realistic beam model.

C. Excitation by a tri-Gaussian beam

Let us apply these results to the case of a non-pencil beam, employing a tri-Gaussian as a simple stand-in for more realistic beam profiles. The beam current density takes the form

$$J_b(x,y,t) = \frac{I_b(t)}{2\pi\sigma_x\sigma_y} \exp\left(-\frac{(x-x_b)^2}{2\sigma_x^2} - \frac{(y-y_b)^2}{2\sigma_y^2} \right), \qquad (35)$$

with current waveform

$$I_b(t) = \frac{Q_b}{(2\pi)^{1/2}\sigma_t} \exp\left(-\frac{(t-t_b)^2}{2\sigma_t^2} \right), \qquad (36)$$

and beam arrival time at $t=0$ is t_b. This beam we view as a superposition of ''pencil beams'', and the induced cavity voltage is accordingly a superposition of the induced voltage from each. Thus in Eq. (25) X_λ is replaced with $\langle X_\lambda \rangle$, where $\langle ... \rangle$ denotes a charge-weighted average over the beam cross-section; to compute this average, we require the various beam moments, involving integrals of the form

$$\langle x^m \rangle = \frac{1}{(2\pi)^{1/2}\sigma_x} \int_{-\infty}^{+\infty} dx \, x^m \exp\left(-\frac{(x-x_b)^2}{2\sigma_x^2} \right), \qquad (37)$$

and using the binomial theorem, and Gaussian integrals, we find $\langle x \rangle = x_b$, $\langle x^2 \rangle = x_b^2 + \sigma_x^2$, $\langle x^3 \rangle = x_b^3 + 3\sigma_x^2 x_b$, $\langle x^4 \rangle = x_b^4 + 6\sigma_x^2 x_b^2 + 3\sigma_x^4$, and $\langle x^5 \rangle = x_b^5 + 15 x_b \sigma_x^4 + 10 x_b^3 \sigma_x^2$, with similar expressions for y. In this way, we obtain $\langle \tilde{w} \rangle = \langle \tilde{w} \rangle_{0,1,2} + \langle \tilde{w} \rangle_3 + \langle \tilde{w} \rangle_4 + \langle \tilde{w} \rangle_5 + \cdots$, where terms through second order are

$$\langle \tilde{w} \rangle_{0,1,2} = b_0 - a_1 y_b + b_1 x_b - 2a_2 x_b y_b$$
$$+ b_2(x_b^2 + \sigma_x^2 - y_b^2 - \sigma_y^2), \qquad (38)$$

sextupole terms are

$$\langle \tilde{w} \rangle_3 = -a_3 y_b[(3x_b^2 - y_b^2) + 3(\sigma_x^2 - \sigma_y^2)] + b_3 x_b[(x_b^2 - 3y_b^2)$$
$$+ 3(\sigma_x^2 - \sigma_y^2)], \qquad (39)$$

octupole terms are

$$\langle \tilde{w} \rangle_4 = -4a_4 y_b x_b[(x_b^2 - y_b^2) + 3(\sigma_x^2 - \sigma_y^2)] + b_4[(x_b^4 - 6x_b^2 y_b^2$$
$$+ y_b^4) + 6(x_b^2 - y_b^2)(\sigma_x^2 - \sigma_y^2) + 3(\sigma_x^2 - \sigma_y^2)^2], \qquad (40)$$

and decapole terms are

$$\langle \tilde{w} \rangle_5 = -a_5 y_b[(y_b^4 - 10x_b^2 y_b^2 + 5x_b^4) + 15(\sigma_x^2 - \sigma_y^2)^2$$
$$- 10(y_b^2 - 3x_b^2)(\sigma_x^2 - \sigma_y^2)] + b_5 x_b[(x_b^4 - 10x_b^2 y_b^2$$
$$+ 5y_b^4) + 15(\sigma_x^2 - \sigma_y^2)^2 + 10(x_b^2 - 3y_b^2)(\sigma_x^2 - \sigma_y^2)]. \qquad (41)$$

These results permit us to evaluate explicitly the beam coordinate function $\langle X \rangle$.

For a predominantly monopole mode, $\langle X \rangle$ amounts to position-dependent correction to the inferred beam charge and phase,

$$\langle X \rangle \approx 1 + B_2^*(x_b^2 - y_b^2 + \sigma_x^2 - \sigma_y^2), \qquad (42)$$

at first order. For a predominantly x-dipole mode,

$$X_b \approx x_b + x_b B_3^*(x_b^2 - 3y_b^2 + 3\sigma_x^2 - 3\sigma_y^2), \qquad (43)$$

at first order.

Next let us solve Eq. (25) explicitly to determine the waveform emitted into the connecting waveguide, to be observed ''upstairs''. We integrate Eq. (25) for a Gaussian current profile, with $V_F = 0$ corresponding to no drive, and a perfectly matched or isolated output load. One may check, by differentiation, that

$$V_{c\lambda}(t) = -2k_{l\lambda} \int_{-\infty}^t dt' \, g(t-t')[I_b\langle X \rangle]_{t'}$$

$$= -2k_{l\lambda}\mathcal{R}\left(1 + j\frac{V_\lambda}{2\Omega_\lambda} \right) e^{-\Gamma_\lambda t} \int_{-\infty}^t dt' \, e^{\Gamma_\lambda t'} [I_b\langle X_\lambda \rangle]_{t'}$$

is the solution of Eq. (25), where we abbreviate $\nu_\lambda = \omega_\lambda/Q_{L\lambda}$, $\Omega_\lambda^2 = \omega_\lambda^2 - \frac{1}{4}\nu_\lambda^2$, $\Gamma_\lambda = \frac{1}{2}\nu_\lambda - j\Omega_\lambda$, and the Green's function is

$$g_\lambda(t) = \left\{ \cos\Omega_\lambda t - \frac{\nu_\lambda}{2\Omega_\lambda}\sin\Omega_\lambda t \right\} e^{-\nu_\lambda t/2}$$

$$= \mathcal{R}\left[\left(1 + j\frac{\nu_\lambda}{2\Omega_\lambda} \right) e^{-\Gamma_\lambda t} \right].$$

Our interest here is not the variation of the cavity voltage during the bunch transit, rather the amplitude and phase at which a cavity mode is ringing, after the bunch has passed. Assuming that the beam transverse coordinates are constant throughout the bunch, and that bunch length is short compared to the mode period, we find

$$V_{c\lambda}(t) = -2k_{l\lambda}Q_b\langle X_\lambda \rangle \exp(-\tfrac{1}{2}\omega_\lambda^2\sigma_t^2)\mathcal{R}\eta_\lambda e^{-\Gamma_\lambda(t-t_b)}, \qquad (44)$$

where

$$\eta_\lambda = \left(1 + j\frac{\nu_\lambda}{2\Omega_\lambda} \right) \exp(-\tfrac{1}{2}j\nu_\lambda\Omega_\lambda\sigma_t^2),$$

and $\eta_\lambda \approx 1$ to an excellent approximation for $Q_{L\lambda} \gg 1$. Thus one sees that after bunch passage, the cavity rings at the resonance frequency Ω_λ (with damping correction). It is helpful to write Eq. (44) as

$$V_{c\lambda}(t) = \mathcal{R}e^{j\Omega_\lambda(t-t_b)}\tilde{V}_{c\lambda}(t), \qquad (45)$$

where the phasor $\tilde{V}_{c\lambda}(t)$ has a step-rise and exponential decay,

$$\tilde{V}_{c\lambda}(t) = -\hat{V}_{c\lambda}H(t-t_b)\exp{-\tfrac{1}{2}\nu_\lambda(t-t_b)}, \tag{46}$$

with amplitude

$$\hat{V}_{c\lambda} = 2k_\lambda Q_b \langle X_\lambda \rangle \eta_\lambda \exp(-\tfrac{1}{2}\omega_\lambda^2 \sigma_t^2). \tag{47}$$

This is just the cavity phasor in the ''rotating frame'', stripped of the high-frequency modulation, and evanescence, and referred to beam phase. It conveys the beam charge, the *form factor* $F_t = \exp(-\tfrac{1}{2}\omega_\lambda^2 \sigma_t^2)$, and the position dependence in $\langle X \rangle$. These dependences on beam moments may be summarized in terms of a generalized form factor. Specifically, for a monopole mode, $\hat{V}_{c\lambda} = 2k_{l\lambda}Q_b F_\lambda \eta_\lambda$, where $F_\lambda = F_l F_t$ and

$$F_l \approx 1 + B_2^*(x_b^2 - y_b^2 + \sigma_x^2 - \sigma_y^2). \tag{48}$$

For an x-dipole mode, $\hat{V}_{c\lambda} = 2k_{\perp\lambda}Q_b F_\lambda \eta_\lambda x_b$, where $F_\lambda = F_\perp F_t$ and

$$F_\perp \approx 1 + B_3^*(x_b^2 - 3y_b^2 + 3\sigma_x^2 - 3\sigma_y^2). \tag{49}$$

To relate these results to observable quantities, note that energy deposited in the cavity by a single bunch is

$$U_\lambda = \frac{|\hat{V}_{c\lambda}|^2}{\omega_\lambda [R/Q]_\lambda} = k_\lambda Q_b^2 |\langle X_\lambda \rangle|^2 \exp(-\omega_\lambda^2 \sigma_t^2), \tag{50}$$

and the power waveform radiating from the cavity rises as a step function, and decays exponentially with e-folding time $T_f/2 = 1/\nu_\lambda = Q_L/\omega_\lambda$. Cavity heating is determined by peak power dissipated in the cavity walls, $P_d = \omega_\lambda U/Q_{w\lambda}$. The peak power radiated out of the cavity is

$$-P_w = \frac{|V_c|^2}{Q_{c\lambda}[R/Q]_\lambda} = \frac{\omega_\lambda}{Q_{e\lambda}}U = \frac{2\beta}{1+\beta}\frac{U}{T_f}. \tag{51}$$

Thus for a monopole mode, we have

$$-P_w = \frac{2\beta}{1+\beta}\frac{1}{T_f}k_{l\lambda}Q_b^2|F|^2 \tag{52}$$

and for a dipole mode,

$$-P_w = \frac{2\beta}{1+\beta}\frac{1}{T_f}k_{\perp\lambda}Q_b^2 x_b^2|F|^2. \tag{53}$$

D. Excitation by a bunch train

To determine the transient signal produced by a bunch train, we superimpose the transient voltages induced by the individual bunches. We number bunches $n = 0,1,..., N-1$, and refer to time t_{bn} the arrival time of the nth bunch (just like the variable t_b used previously), so that t_{b0} is the arrival time of the lead bunch. Let us express the timing of the nth bunch with respect to bunch #0 as $\tau_n = t_{bn} - t_{b0}$. For typical accelerator operation, the bunch spacing is approximately constant, $\tau_n - \tau_{n-1} \approx 2\pi/\Omega_0$, where Ω_0 corresponds to the angular frequency for the accelerator, or a subharmonic of it. For definiteness, we will suppose the former. In general Ω_0 may differ from the mode resonance frequency Ω_λ, in the case of a cavity temperature excursion, or for a parasitic, nonresonant mode.

The voltage waveform induced by the nth bunch is

$$V_{c\lambda n}(t) = \mathcal{R}e^{-\Gamma_\lambda(t-t_{bn})}H(t-t_{bn})\hat{V}_{c\lambda n}, \tag{54}$$

where

$$\hat{V}_{c\lambda n} = 2k_\lambda Q_{bn}\langle X_{\lambda n}\rangle \exp(-\tfrac{1}{2}\omega_\lambda^2 \sigma_{tn}^2). \tag{55}$$

We may then express the total voltage at any time as

$$V_{c\lambda}(t) = \sum_{n=0}^{N-1} V_{c\lambda n}(t) = \mathcal{R}\sum_{n=0}^{t_{bn}<t} e^{-\Gamma_\lambda(t-t_{bn})}\hat{V}_{c\lambda n}$$

$$= \mathcal{R}e^{-\Gamma_\lambda(t-t_{b0})}\sum_{n=0}^{t_{bn}<t} e^{\Gamma_\lambda \tau_n}\hat{V}_{c\lambda n}. \tag{56}$$

The latter sum is taken over those bunches that have already passed as of time t. This sum may be employed to study analytically and numerically the effects of systematics due to τ_n, F_n, and Q_{bn} variations with n. For numerical studies, computation of the sum in Eq. (56) is amenable to a recursive form; we evaluate our sum just after the passage of the mth bunch, rearranging it to find

$$\tilde{V}_{c\lambda}(t_{bm+}) = \hat{V}_{c\lambda m} + e^{-\Gamma_\lambda(\tau_m \tau_{m-1})}\tilde{V}_{c\lambda}(t_{bm-1+}). \tag{57}$$

This series starts after the 0th bunch, with $\tilde{V}_{c\lambda}(t_{b0+}) = \hat{V}_{c\lambda 0}$.

An explicit analytic result is instructive and is easily obtained in the case of an idealized ''top-hat'' current profile, a uniformly bunched beam, steady or small beam size along the bunch train, and steady or small centroid offset along the train. We permit a frequency deviation between the beam and cavity resonance. Summing a geometric series, we find

$$V_{c\lambda}(t) = \mathcal{R}\exp[\Gamma_\lambda(t-t_{b0})]\hat{V}_{c\lambda 0}\frac{\exp(\Gamma_\lambda \tau n)-1}{\exp(\Gamma_\lambda \tau)-1}, \tag{58}$$

where n indexes the last bunch that passed, i.e., $t_{bn} < t < t_{bn+1}$. At early times this gives a voltage waveform rising linearly in time and output power rising quadratically. As time goes on, the system reaches a steady state between power deposited by the beam, and power absorbed by the walls, and radiated down the waveguide. After the bunch train has gone by, the voltage decays exponentially.

In the case of a cavity perfectly tuned to resonance with the perfectly bunched beam, we have $\Gamma_\lambda \tau = \nu_\lambda \tau/2 = \pi/Q_{L\lambda} \ll 1$, and

$$V_{c\lambda}(t) \approx \mathcal{R}\exp^{j\Omega_\lambda(t-t_{b0})}\frac{\hat{V}_{c\lambda 0}}{\Gamma_\lambda \tau} = \mathcal{R}\exp^{j\Omega_\lambda(t-t_{b0})}\hat{V}_{\text{eff},\lambda}, \tag{59}$$

where

$$\hat{V}_{\text{eff},\lambda} = \frac{Q_{L\lambda}}{\pi}\hat{V}_{c\lambda 0} = -2k_\lambda Q_{b\text{eff},\lambda}\langle X_\lambda\rangle \exp(-\tfrac{1}{2}\omega_\lambda^2 \sigma_t^2) \tag{60}$$

and $Q_{b\text{eff},\lambda} = Q_{L\lambda}Q_b/\pi$ is the amount of charge passing through the cavity in one fill time. This may also be expressed as $\hat{V}_{\text{eff},\lambda} = I_b R_{L\lambda}\langle X_\lambda\rangle \exp(-\tfrac{1}{2}\omega_\lambda^2 \sigma_t^2)$, where $I_b = \Omega_0 Q_b/2\pi$ is the intrapulse current, and the loaded shunt impedance $R_{L\lambda} = Q_{L\lambda}[R/Q]_\lambda$ evidently characterizes such steady-state resonant excitation.

Appreciating that the resonant enhancement can be large, let us consider the effect of detuning from resonance.

We parameterize the detuning of the cavity resonance frequency Ω_λ from the bunch train frequency Ω_0 by the tuning angle

$$\tan \psi_\lambda = Q_{L\lambda}\left(\frac{\Omega_\lambda}{\Omega_0} - \frac{\Omega_0}{\Omega_\lambda}\right) \approx 2 Q_{L\lambda}\left(\frac{\Omega_\lambda - \Omega_0}{\Omega_0}\right), \qquad (61)$$

in terms of which,

$$V_c(t) \approx \mathcal{R} \exp[j\Omega(t - t_{b0})]\frac{Q_L}{\pi}\hat{V}_{c0}\cos\psi e^{j\psi}. \qquad (62)$$

Evidently tuning error introduces both a phase and an amplitude error. The amplitude error is second order in the tuning angle, and the phase error is just the tuning angle. In general, the amplitude of the resonant denominator in Eq. (61) is

$$\Lambda^{-1} = |e^{\Gamma\tau} - 1| = 2\exp\left(\frac{\pi}{2Q_L}\right)\left[\sinh^2\left(\frac{\pi}{2Q_L}\right) + \sin^2\left(\frac{\pi\Omega}{\Omega_0}\right)\right]^{1/2}, \qquad (63)$$

so that, in the case of large detuning from resonance the enhancement factor of Q_L/π is replaced with a factor of order unity.

Before leaving the matter of bunch train excitation, let us note an alternative method of computing the transient cavity voltage. We approximate our expression for beam current using the first-harmonic component, $I_{b0} \approx \mathcal{R}\widetilde{I}_{b0}e^{j\omega t}$, and similarly represent the cavity voltage as $V_c \approx \mathcal{R}\widetilde{V}_c e^{j\omega t}$. We make the slowly varying envelope approximation, such that $|d\widetilde{I}_{b0}/dt| \ll \omega|\widetilde{I}_{b0}|$, and find

$$\frac{d\widetilde{V}_c}{dt} + \frac{1}{T_f}(1 - j\tan\psi)\widetilde{V}_c \approx -k_l\widetilde{I}_{b0}.$$

Abbreviating $\Delta = (1 - j\tan\psi)/T_f$, one finds that for an initially unexcited cavity, and a beam current waveform arriving at $t = 0$,

$$\widetilde{V}_c(t) \approx -k_l e^{-\Delta t}\int_0^t dt'\widetilde{I}_{b0}(t')e^{\Delta t'}.$$

Using $\widetilde{I}_b = 2I_b F_t$ one confirms the result obtained from superposition of single bunches.

This completes our analysis of the interaction of the beam with the waveguide-coupled cavity modes. In the next section, we illustrate these considerations for an example beam-position monitor system.

III. TWO-CAVITY BPM SYSTEM

We consider the beam-position monitor system illustrated in Fig. 3, as discussed in Ref. 1. The system makes use of three cavities, including a vertical position monitor cavity; however, without loss of generality, we are free to concentrate on analysis of beam-position monitoring in the horizontal.

A. Phase cavity

The geometry of the phase cavity is seen in Fig. 4 as originally designed by Altenmueller and Brunet.[10] One can appreciate the parameters for the phase cavity with reference to the scalings for a closed, cylindrical pillbox—the cavity prior to perturbation by the beam port, nose cones, and external coupling. In this idealized model, optimum shunt im-
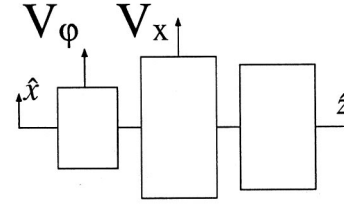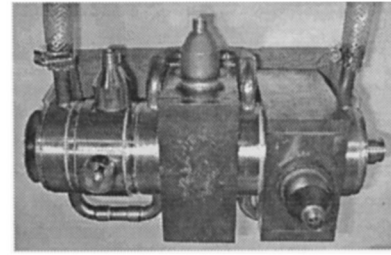

FIG. 3. This 12 in.-long assembly consists of three 2856 MHz cavities for monitoring of beam phase, and horizontal and vertical position. We will analyze the combination of the x cavity and the phase cavity.

pedance occurs for $\theta = 158.1°$ and is $R_s \approx 3.77\,\text{M}\Omega$, with $Q_w \approx 1.73\times10^4$, and $[R/Q] \approx 220\,\Omega$. A more precise result is obtained with an electromagnetic field solver and we employ the finite difference code $GdfidL$.[11] We obtain $f \approx 2836\,\text{MHz}$, $Q_w \approx 1.51\times10^4$, $[R/Q] \approx 236\,\Omega$, and $k_l \approx 1.11\,\text{V/pC}$. Given the accessibility of the cavities for bench measurement, the analytic scalings and the electromagnetic computations are primarily of use for mode identification, and accurate calculation of the mode coupling coefficients a_n, b_n.

Characteristics of the phase cavity have been measured on the bench as part of a three-cavity assembly, as seen in Fig. 3, employing an HP8510 vector network analyzer, with N-type calibration and 801 points over a span of 20 MHz. Cavity temperature was held steady to $0.5°\text{C}$ by means of temperature-stabilized water flow. We find $f \approx 2855.8\,\text{MHz}$ at $T = 45.0°\text{C}$, with temperature coefficient of $df/dT \approx -6\times10^4\,\text{Hz/°C}$. Inferred $Q_w \approx 7.9\times10^4$, while Q_L was found to be sensitive to the state of the connector.

Comparing these figures to those of Altenmueller and Brunet, their value $Q_L \approx 1200$ is consistent. Their estimate $[R/Q] \approx 248\,\Omega$ is about 5% higher. For a loaded shunt impedance of $R_s \approx 0.28\,\text{M}\Omega$, and loaded fill time $T_f = 2Q_L/\omega \approx 133\,\text{ns}$, the single-bunch scalings are $U \approx 1.1\,\mu\text{J}\,Q_b^2(\text{nC})$, and $P_w \approx 15\,\text{W}\,Q_b^2(\text{nC})$. The steady-state, multibunch scaling is obtained with the substitution $Q_b \to Q_{b\text{eff}} = Q_L Q_b/\pi$, and corresponds to $P_w \approx 0.26\,\text{W}\,I_b^2(\text{mA})$.

For this phase cavity, we have cylindrical symmetry to an excellent approximation, so that the quadrupole term $b_2 \approx 0$. In fact, even a slight quadrupole component would not significantly effect the systematics of this signal, since it is not employed near a signal null, unlike the position cavity. One might be concerned about the bunch-length dependence of the cavity emitted signal, insofar as pulse-to-pulse fluctuation in (unmonitored) bunch length could then function as a source of ''noise''. Two features mitigate against this potential systematic however. First, the bunch length typically must be quite small, insofar as a long bunch will exhibit energy spread unacceptable for experimental application of the beam. The root-mean-square (rms) phase width of the
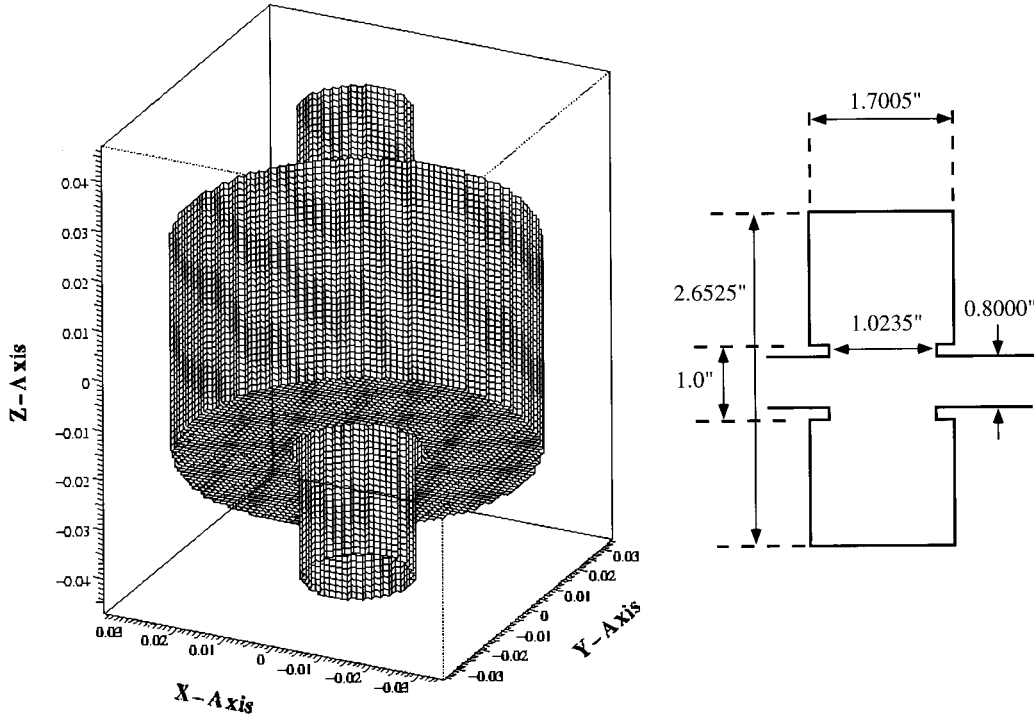
FIG. 4. Interior dimensions for the beam-phase monitor cavity and the geometry as employed in the field solver.

beam $\sigma_\psi(°\mathrm{rf}) \approx 6.8\sqrt{\delta_E(\%)}$ with δ_E the rms energy spread. Thus even if the accelerator is configured to produce a large rms energy spread of say 1%, the bunch length will be short, less than 2.0 mm. In this case, $\exp(-\frac{1}{2}\omega_\lambda^2\sigma_t^2) \approx 0.993$, and the form factor correction must necessarily be small. Fluctuation in the form factor correction is then an even smaller effect, negligible for applications we can envision. The second factor mitigating against bunch-length induced jitter arises when the signal-processing scheme employs the beam-induced phase-signal to normalize the beam-induced position signal. In this case, the form-factor correction for bunch length divides out, leaving a result independent of bunch length. This is seen in the analysis of Sec. IV.

B. Position cavity

The resonant beam-position monitor cavity is depicted in Fig. 5, as originally designed by Brunet *et al.*[12] We consider analysis of horizontal position for definiteness, as a similar analysis applies to the vertical. We could add that the actual degree of freedom one is looking at depends on the alignment during installation. To appreciate the fields and coupling of the position cavity, one may consult in the first approximation, the closed-pillbox geometry. For beam and cavity axis perfectly parallel, the beam couples only to TM modes of the pillbox (those with an axial electric field). The lowest frequency modes are the TM_{mn0} modes (no longitudinal variation in axial electric field), with field components

$$E_z = \widetilde{E}_0 \sin(\beta_x x)\sin(\beta_y y),$$

$$Z_0 H_x = j\frac{\beta_y}{\beta_0}\widetilde{E}_0 \sin(\beta_x x)\cos(\beta_y y),$$

$$Z_0 H_y = -j\frac{\beta_x}{\beta_0}\widetilde{E}_0 \cos(\beta_x x)\sin(\beta_y y),$$

where other components zero. The coordinates relative to the beam axis are $x_1 = x - d/2$ and $y_1 = y - a/2$, where $a = 4.1820$ in. $= 10.6223$ cm, is the cavity height, and $d = 4.7080$ in. $= 11.9583$ cm is the cavity width. Cavity length is $b = 2.001$ in. $= 5.0825$ cm. Wave numbers are $\beta_x = m\pi/d$, $\beta_y = n\pi/a$, and $\beta_0 = \sqrt{\beta_x^2 + \beta_y^2}$. The resonant angular frequency is $\omega_0 = c\beta_0$. In this notation, the ''accelerating mode'' or ''monopole mode'' is TM_{110}, and the first two ''position sensitive'' or ''dipole modes'' are TM_{210} and TM_{120}.

Using these modal fields one can show that for the design TM_{210} mode (x-dipole mode),

$$k_\perp = \frac{1}{x^2}\frac{\omega_0}{4}\left[\frac{R}{Q}\right]_{(x,0)} \approx (2cZ_0)T^2\left(\frac{\beta_x^2 b}{ad}\right) \tag{64}$$

and

$$\frac{1}{Q_w} = \frac{\delta}{2}\frac{\int dS|\widetilde{H}|^2}{\int dV|\widetilde{H}|^2} = \frac{2\delta}{\beta_0^2}\left(\frac{\beta_x^2}{d} + \frac{\beta_y^2}{a} + \frac{\beta_0^2}{2b}\right), \tag{65}$$

where the skin-depth $\delta \approx 2.1\ \mu\mathrm{m}/\sqrt{f(\mathrm{GHz})} \approx 1.2\ \mu\mathrm{m}$ for copper. The corresponding frequency is 2.8768 GHz. Theoretical wall Q is $Q_w \approx 2.26\times 10^4$. Transit angle is 199°, corresponding to transit angle factor $T = \sin(\theta/2)/(\theta/2) \approx 0.568$. Then $k_\perp \approx 8.07\times 10^{-2}$ V/pC cm^2, $[R_\perp/Q] \approx 17.8\ \Omega$ cm^{-2}, and $R_\perp \approx 4.0\times 10^5\ \Omega/\mathrm{cm}^2$.

In addition to the design mode, the monopole mode, TM_{110} will be excited by the beam. Unlike the TM_{210} position mode, the TM_{110} mode has nonzero reading with beam centered, and thus acts as a common mode between different position readings. This is a concern since the output coupling
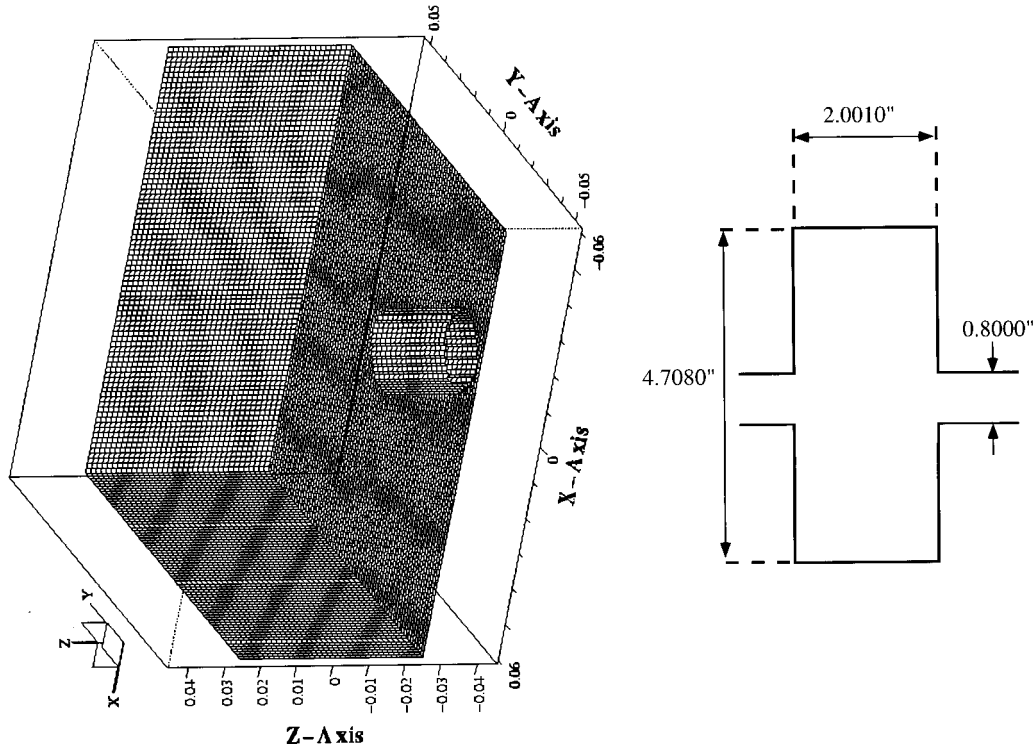
FIG. 5. Interior dimensions for a horizontal position cavity, and the geometry as employed in the field solver.

is asymmetric and unable to distinguish the two modes by symmetry, as seen in Fig. 6. The natural correction to this problem, is to employ two outputs coupled through a hybrid tee, to remove modes of even symmetry, up to the isolation provided by the tee. In the meantime, the implication for the output waveform from the cavity is that it includes a finite contribution from a monopole mode, due to the finite external Q of that mode. To estimate the excitation of the TM_{110} mode, we employ closed-pillbox scalings and find a resonant frequency of $f_M = 1.8875 \, \text{GHz}$ and $Q_w \approx 1.66 \times 10^4$. Transit angle is $115°$ and the transit angle factor is $T \approx 0.84$, so that

$$\left[\frac{R}{Q}\right] = Z_0 T^2 \left(\frac{8b}{\beta_0 a d}\right) \approx 215 \, \Omega, \tag{66}$$

and loss factor is $k_l \approx 0.64 \, \text{V/pC}$. We note that there is also a y-dipole mode, TM_{120} at 3.088 GHz; however, symmetry hinders its coupling to the guide.

To obtain more precise results, and to accurately determine the higher-order dependence on transverse position, we employ the field-solver. Results are summarized in Table II. The monopole mode frequency $f \approx 1893 \, \text{GHz}$, with $Q_w \approx 1.72 \times 10^4$, $[R/Q] \approx 196 \, \Omega$, and $k_l \approx 0.88 \, \text{V/pC}$. The higher multipole content of this mode is of interest in connection with the BPM offset. Given the symmetry of the cavity, we expect to find
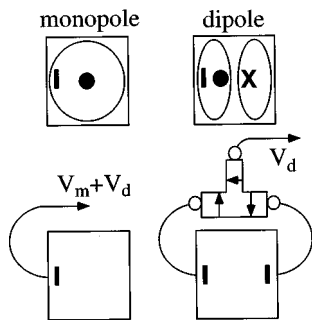

FIG. 6. Illustration of monopole mode coupling to a single output, and suppression of the monopole mode by means of two outputs. The sign of the integrated electric field is indicated by the solid dots and the cross; magnetic field lines correspond to the circles; the beam passes into the page. Use of symmetric couplers and a tee separates modes of opposite symmetry.

TABLE II. The first few modes of the linac position cavity.

Mode	f(MHz)	$Q_w(\times 10^4)$	type
1	1893	1.72	monopole
2	2861	2.17	x dipole (design)
3	3071	2.18	y dipole
4	3183	1.90	hybrid y dipole
5	3247	1.98	hybrid x dipole
6	3499	1.74	
7	3505	1.54	monopole
8	3771	2.44	
9	3867	2.37	
10	4029	2.42	monopole
11	4077	2.44	
12	4193	1.79	
13	4251	1.97	
14	4418	2.61	monopole
15	4757	2.55	

$$\left[\frac{R}{Q}\right]\approx\left[\frac{R}{Q}\right]_0 |1+B_2(x^2-y^2)+B_4(x^4-6x^2y^2+y^4)$$

$$+O(r_\perp^6)...|^2. \tag{67}$$

Analysis of the solver output leads to a fit for the normal quadrupole and normal octupole components, $B_2\approx6.3\times10^{-3}$ cm^{-2}, $B_4\approx-5.7\times10^{-3}$ cm^{-4}.

The mode near 2856 MHz is the intended operating mode for the cavity. Evidently the cutting of the beam port (where magnetic field is large, and electric field small) lowers the frequency from the closed pillbox estimate. This mode falls into the category of an ''odd in x, even in y'' mode and so we may expect to find

$$\left[\frac{R}{Q}\right]\approx x^2\left[\frac{R_\perp}{Q}\right]|1+B_3(x^2-3y^2)+B_5(x^4-10x^2y^2+5y^4)$$

$$+O(r_\perp^6)...|^2. \tag{68}$$

Analysis with the field solver shows that $Q_w\approx2.17\times10^4$, $[R_\perp/Q]\approx23.2\,\Omega$ cm^{-2}, $k_\perp\approx1.04\times10^{-1}$ V/pC cm^2, $B_3\approx-4.2\times10^{-3}$ cm^{-2}, and $B_5\approx-4.4\times10^{-3}$ cm^{-4}. The fit agrees to three digits in most cases, except for offsets approaching 1 cm, where agreement is to two digits. In practical terms, for a 1 mm offset these terms amount to a correction at the level of 100 ppm in beam-induced voltage, and will be completely negligible. Given that the beam pipe radius is 1 cm, the maximum correction one could produce (if one were trying) would be at the level of 1% in voltage, at the cost of scraping beam in the aperture.

The y-dipole mode appears at 3017 MHz, with $[R_\perp/Q]\approx22.8\,\Omega$ cm^{-2}. Mode #4, at 3184 MHz is also a y-dipole mode, a hybrid derived from the lowest TE mode of the closed pillbox, TE$_{101}$. This mode has a vertical electric field developing a longitudinal component due to the beam ports, with a resulting odd symmetry in y, and even symmetry in x. It has a low $[R_\perp/Q]\approx0.3\,\Omega$ cm^{-2}, as does the 3247 MHz x-dipole hybrid with $[R_\perp/Q]\approx0.4\,\Omega$ cm^{-2}, derived from the TE$_{011}$ mode.

One additional mode, #35, is noteworthy in that it is close to a beam harmonic. It is a y-dipole mode at at 8592 MHz with $[R_\perp/Q]\approx0.7\,\Omega$ cm^{-2}. If the mode of the actual cavity (as opposed to our numerical model) were in fact 24 MHz away from the 3×2856 MHz=8568 MHz beam harmonic, this would be no cause for concern. However, at this level of precision one would prefer to check the actual cavity to see where the mode lies, after perturbations due to the coupler, brazing, dimpling, vacuum, and temperature.

We performed bench measurements on the position cavity under conditions as in Sec. III A, finding for the design mode a temperature coefficient of $df/dT\approx-5\times10^4$ kHz/°C, and $f=2854.4$ MHz at $T=45.0$ °C. From measurement of S_{11} we infer $Q_L\approx6.5\times10^2$ and $\beta\approx16.5$, so that $Q_w\approx1.1\times10^4$. These parameters correspond to a loaded transverse shunt impedance of $R_{\perp L}\approx1.5\times10^4\,\Omega$ cm^{-2} and fill-time $T_f\approx72$ ns. For the first parasitic mode, the monopole mode, $f\approx1890.1$ MHz at $T=45.0$ °C, tuning with temperature as $df/dT\approx-1\times10^5$ kHz/°C. We find $Q_L\approx2.9\times10^3$ and $\beta\approx3.6$, corresponding to $Q_w\approx1.3\times10^4$, $R_L\approx0.6$ MΩ, and $T_f\approx0.32\,\mu$s. A survey of modes near the

first three beam harmonics shows a low-Q coupler resonance 24 MHz below the 5712 MHz harmonic, a cavity mode 8 MHz below the 8568 MHz harmonic, and a mode 3 MHz above the 11 424 MHz harmonic. This last mode, and any higher parasitic, near-harmonic modes will not be cut off in the beam tube, and thus accurate assessment of their frequency and width is best determined from beam-based observations. In the meantime, it would be prudent in operation to remove such harmonics by filtering. In the setup of Fig. 3, cross-talk between the phase cavity and the adjacent x cavity may be quantified by measurement of S_{12} between the two output couplers, and is less than -70 dB, and not accessible with our calibration. This good isolation we attribute to the symmetry of the modal field patterns, and the high beam-tube cut-off frequency of 8.65 GHz.

With mode parameters in-hand, we compute that a single-bunch deposits energy $U\approx1.0$ nJ Q_b^2(nC)x_b^2(mm) in the design mode, corresponding to $P_w\approx27$ mW Q_b^2(nC)x_b^2(mm). In steady state, this takes the form $P_w\approx0.14$ mW I_b^2(mA)x_b^2(mm). For the parasitic monopole mode, $P_w\approx4.3$ W Q_b^2(nC) for a single bunch.

Next, we consider the concerns arising in analysis of the multimode waveform emitted by a beam-excited cavity. We will employ the BPM cavities and characteristics described in this section for numerical examples.

IV. POSITION MEASUREMENT

To appreciate the effect of higher-mode and multipole systematics in inference of position, a model for the signal processing is required. In this section, we first make some simple estimates based on signal amplitudes, and then go on to consider phase information as well. We employ an idealized model for signal processing, assuming linearity, infinite dynamic range, no digitization error, and, where downmixing is invoked, a stable, tuned local oscillator, with at most a constant phase error.

A. Signal levels

Let us suppose in the simplest (and worst) case, that one performs power detection on the output of the x-cavity signal. If one attempts to estimate the resolution in single-bunch mode by comparing energy deposited in the dipole and monopole modes one arrives at a position $x_b\approx\sqrt{k_{lm}/k_{\perp d}}\approx2.9$ cm, lying outside the beam pipe. If one filters the output, the parasitic mode amplitude is reduced by a factor of order $1/Q_L$, and becomes comparable to the dipole signal at offsets on the order of $x_b\approx O(10\,\mu$m). The situation can be improved further by symmetric output coupling as depicted in Fig. 6, or a variant as seen in Fig. 7. With the monopole mode amplitude reduced by a factor of ϵ, the signals become comparable at $x_b\approx O(10\,\mu$m)ϵ, and beam motion at the 1 μm level could be resolved easily. For a bunch train, excitation of the off-resonance parasitic mode results in signal reduction, below the level for a single bunch, by a factor $\Lambda\approx O(1)$, from Eq. (63); meanwhile, the design-mode amplitude is enhanced by the factor Q_{L0}/π. For our parameters this implies comparable signal levels at $x_b\approx O(10^2\,\mu$m). In this bunch-train mode of operation, filtering helps to remove
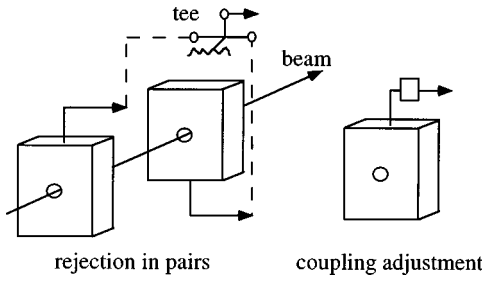
FIG. 7. Options for retrofitting of existing cavity BPMs to improve performance include coupling adjustment with an in-line tuner, and combining of two adjacent cavity outputs in a hybrid tee to subtract the monopole mode contribution.

harmonics, but not the driven oscillation at the beam fundamental frequency. With symmetrized output coupling, one could obtain $x_b \approx O(5 \ \mu m)$; this figure can be reduced into the submicron range, if the dipole mode coupling is adjusted, as seen in Fig. 7, to raise the loaded Q.

In light of the foregoing discussion one is naturally inclined, where precision is required, toward subtraction of the parasitic mode signal. This is best accomplished employing phase information, and vector subtraction. This may be illustrated most simply referring to the integral of the down-mixed waveform corresponding to the parasitic mode,

$$\int_{-\infty}^{+\infty} dt \, \tilde{V}_{c-CM}(t) e^{j\Delta\Omega(t-T)} \approx \frac{R_{L-CM}Q_b}{1-jT_{f-CM}\Delta\Omega},$$

with R_{L-CM} the loaded shunt impedance of the parasitic mode, T_{fCM} the fill time, and $\Delta\Omega_{CM} = \Omega_{CM} - \Omega_0$ the detuning of the parasitic mode from resonance with the bunch train. Taking $\Omega_{CM} \approx 2\pi \times 1.89$ GHz, $\Omega_0 \approx 2\pi \times 2.856$ GHz, and $T_{fCM} \approx 100$ ns, one has $T_{fCM}\Delta\Omega \approx 6.1 \times 10^2$, as one would obtain from Eq. (63). The feature to note about this result is that the phase of this signal is fixed with respect to the beam, and independent of offset. Thus if a reliable phase reference is available at the waveguide output ''upstairs'' (for example, derived from the phase cavity), the parasitic-mode component can be balanced out in a tee. Assuming a common cable run, and roughly equal cable lengths, this may be achievable in a diurnally reliable fashion. In the case that consistent monitoring is required over a scale only of minutes, requirements are relaxed. With these considerations in mind, let us consider in a detail a more elaborate use of phase information.

B. Scale and offset

We consider a front-end processor as depicted in Fig. 8, employing a free-running local oscillator (LO) and a dual
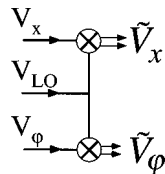

FIG. 8. We analyze systematics as they would appear at the output of a homodyne dual mixer providing in-phase and quadrature waveforms, followed by integration on each channel.

output (in-phase and quadrature) mixer. We can express the voltage phasors from the position and phase cavities, as they would after down-mixing and detection,

$$\tilde{V}_\varphi = c_\varphi Q_{eff} e^{j\phi}, \tag{69}$$

$$\tilde{V}_x = c_x Q_{eff} x_b + \epsilon_x Q_{eff}. \tag{70}$$

The term ϵ_x represents the parasitic mode component. The phase ϕ we introduce to account for any phase error incurred in the signal processing, e.g., differential cable expansion or differential phase drift between the LO used for the x-cavity signal, and that for the phase-cavity signal. The coefficients c_x, c_φ are determined from calculations in the foregoing sections, and cable propagation characteristics. The effective charge Q_{eff}, is determined from the convolution of beam current with the cavity response. These parameters are imbued with the choice of sampling technique. We can express the position phasor as

$$\tilde{V}_x = c_x Q_{eff}(x - \tilde{x}_0), \tag{71}$$

where the offset

$$\tilde{x}_0 = -\frac{\epsilon_x}{c_x} = x_{0r} + jx_{0i} \tag{72}$$

is in general complex. Dependence of voltage amplitude on position is given by

$$|\tilde{V}_x|^2 = |c_x Q_{eff}|^2 [(x - x_{0r})^2 + x_{0i}^2], \tag{73}$$

and exhibits both a nonzero minimum and an offset from the center axis defined by the position-sensitive mode.

Analysis of the detected signal permits inference of a result for position given by

$$X = k\mathcal{R} \frac{\tilde{V}_x \tilde{V}_\varphi^*}{\tilde{V}_\varphi \tilde{V}_\varphi^*} = k\mathcal{R} \frac{(c_x x + \epsilon_x)}{c_\varphi e^{j\phi}} = Sx + X_0, \tag{74}$$

with some choice of calibration constant k. Thus the response of such a BPM is determined from the scale, and the intercept,

$$S = k\mathcal{R} \frac{c_x}{c_\varphi} e^{-j\phi} \quad \text{(BPM scale factor)}, \tag{75}$$

$$X_0 = k\mathcal{R} \frac{\epsilon_x}{c_\varphi} e^{-j\phi} \quad \text{(BPM intercept)}. \tag{76}$$

The intercept corresponds to the reading for a centered beam, and should be distinguished from the offset of the beam at zero reading, $-X_0/S$.

Let us analyze the systematic errors in scale and offset, to characterize the intrinsic resolution of the BPM with this front-end processor. To do so in the most specific fashion, we should indicate by what means the voltage phasors are processed. For simplicity, we will assume that the full voltage waveforms are integrated with gatewidth longer than the pulse length. This manner of detection, has the advantage that the area under the cavity phasor curve is proportional to the pulse-averaged charge (in the case of $\int \tilde{V}_\varphi dt$) or the pulse-averaged, charge-weighted position (in the case of $\int \tilde{V}_x dt$).

We suppose the phase cavity provides a pure monopole cavity phasor $\tilde{V}_{c-\varphi}$. The position cavity provides a cavity

phasor $\tilde{V}_{c-x}$ that is a superposition of a predominantly dipole mode (the design mode), and a predominantly monopole mode (a parasitic mode). In this case,

$$\tilde{V}_\varphi \equiv e^{j\phi} \int_{-\infty}^{+\infty} dt\, \tilde{V}_{c-\varphi}(t) \approx e^{j\phi} R_L \sum_n Q_{bn} F_{\varphi n}, \quad (77)$$

$$\tilde{V}_x \equiv \int_{-\infty}^{+\infty} dt\, \tilde{V}_{c-x}(t) \approx R_{\perp L} \sum_n Q_{bn} x_b F_{xn}$$

$$+ n'' \eta \frac{R_{L-CM}}{1 - j T_{fCM} \Delta\Omega_{CM}} \sum_n Q_{bn} F_{CMn}. \quad (78)$$

The loaded shunt impedances are: R_L for the monopole mode of the phase cavity, $R_{\perp L}$ for the dipole mode of the position cavity, and R_{L-CM} for the parasitic mode of the position cavity. The generalized form factors are F_{xn} for the dipole mode of the position cavity, $F_{\varphi n}$ for the monopole mode of the phase cavity, and F_{CMn} for the parasitic mode of the position cavity. In the last expression, we include a factor η to account for any additional measures employed against the parasitic mode (e.g., symmetrization as in Fig. 6). Using Eq. (34) the magnitude of the offset of Eq. (72) may be expressed up to an overall phase factor as

$$|\tilde{x}_0| \approx \frac{1}{2} \frac{|\eta|}{|\Delta\Omega_{CM}/\Omega_{CM}|} (1 + \beta_x)$$

$$\times \beta_x^{-1/2} \left(\frac{[R/Q]_{CM}}{[R_\perp/Q]_x} \right)^{1/2} (Q_{eCM} Q_{wx})^{-1/2},$$

where we consider a uniform beam and comparable form factors, for illustration. Thus the parasitic-mode offset is minimized for an undercoupled parasitic mode ($\beta_{CM} \to 0$), and a critically coupled dipole mode ($\beta_x = 1$).

Comparing Eqs. (77) and (78) to Eqs. (69) and (70), and neglecting cable propagation factors, we may identify

$$c_\varphi Q_{\text{eff}} \approx R_L \sum_n Q_{bn} F_{\varphi n}, \quad (79)$$

$$c_x Q_{\text{eff}} x \approx R_{\perp L} \sum_n Q_{bn} x_b F_{xn}, \quad (80)$$

$$\epsilon_x Q_{\text{eff}} \approx n'' \eta \frac{R_{L-CM}}{1 - j T_{fCM} \Delta\Omega_{CM}} \sum_n Q_{bn} F_{CMn}. \quad (81)$$

Making use of the the *actual* charge-weighted beam-centroid $x \equiv \Sigma Q_{bn} x_{bn} / \Sigma Q_{bn}$, the scale factor may be expressed as

$$S = \frac{\Sigma Q_{bn} x_{bn} F_{xn}}{\Sigma Q_{bn} \exp F_{\varphi n}} \frac{\Sigma Q_{bn}}{\Sigma Q_{bn} x_{bn}} \cos\phi, \quad (82)$$

where we suppose that the calibration factor has been chosen as $k = R_L / R_{\perp L}$ to make $S = 1$ for $\cos\phi = 1$, and a perfectly centered beam, uniform throughout the pulse. Intercept is given by

$$X_0 \approx \eta n'' \frac{R_{L-CM}}{R_{\perp L}} \frac{\Sigma Q_{bn} F_{CMn}}{\Sigma Q_{bn} \exp F_{\varphi n}} \frac{\sin\phi}{T_{fCM} \Delta\Omega_{CM}}. \quad (83)$$

To illustrate, let us consider the cavity system of Sec. III, and suppose a requirement to resolve 1 μm out of 100 μm.

We must then insure that the scale factor is constant at the level of 1%. For a ''top-hat'' macropulse with no chirp in beam variables, we have

$$S \approx F_\perp \cos\phi \approx [1 + B_3^*(x_b^2 - 3y_b^2 + 3\sigma_x^2 - 3\sigma_y^2)]\cos\phi, \quad (84)$$

with no bunch length dependence. Recall that $B_3 \approx -4.2 \times 10^{-3}\, \text{cm}^{-2}$ is small, with the result that scale deviation due to nonlinearities occurs only for gross vertical misteering of order 9 mm. For scale factor to be constant at the 1% level, we require that ϕ be stable to better than 8°. If the requirement were 0.1% (1 μm out of 1 mm), then ϕ should be stable to better than 2.5°, and vertical misteering should not exceed 2.8 mm. In view of these results maintenance of a reliable scale factor appears feasible.

We must also insure that the intercept is stable to 1 μm over the measurement period. This is the point where one needs to account for the quadrupolar content of the monopole mode of the x cavity. In the previous section, we found that this could be quantified in terms of

$$F_l \approx 1 + B_2^*(x_b^2 - y_b^2 + \sigma_x^2 - \sigma_y^2). \quad (85)$$

The normal quad component for the parasitic mode of the linac-style x cavity was found to be $B_2 \approx 6.3 \times 10^{-3}\, \text{cm}^{-2}$. As a consequence of this quadrupolar component in the parasitic mode, the intercept takes on a dependence on beam coordinates that could in principle disturb the measurement of true position variation. So, for example, let us suppose that operation with a beam motion over a range as large as $x_b \approx 1$ mm is envisioned, and, at the same time it is required that the intercept remain stable at the level of 1 μm. In this case, we require $X_0 B_2 x_b^2 < 1$ μm or $X_0 < 1.6$ cm. Thus the absolute intercept X_0 cannot be too large. We can estimate its magnitude using $R_{L-CM} \approx 0.6\, \text{M}\Omega$, $R_{\perp L} \approx 15\, \text{k}\Omega\, \text{cm}^{-2}$, $|n''| \approx 0.15\, \text{cm}^{-1}$, and $T_f \Delta\Omega \approx -1.9 \times 10^3$. We find $X_0 \approx 30\, \mu\text{m} \times \eta \sin\phi$. This implies that despite the transverse variation in the parasitic mode, and its possible effect in ''faking'' beam motion, one has several orders of magnitude to spare.

Note also that in the case of a macropulse-integrated signal, the effect of equal x-cavity and φ-cavity tuning errors cancel in their contribution to scale error. That is to say that both phasors are multiplied by the same complex correction factor $\cos\psi e^{j\psi}$, and these factors cancel. The residual effect of cavity tuning error in this case is through the parasitic-mode intercept X_0. The parasitic mode, being already greatly detuned, picks up little in the way of a correction in this case. Thus a drift in cavity tune from zero tuning angle to $\delta\psi$, results in a drift in intercept, through the normalization signal,

$$X_0 \approx 30\ \mu\text{m} \times \eta \frac{\sin(\phi + \delta\psi)}{\cos(\delta\psi)}.$$

To hold intercept drift to 1 μm requires control of phase angle at the level of $\delta\psi < 1.9°$. With $Q_L \approx 1200$ for the phase cavity, and temperature detuning of -60 kHz/°C, this implies temperature regulation at the level of 0.5 °C.

To conclude this discussion, let us emphasize that, for the sake of illustration and simplicity, we have made some assumptions regarding the signal processing that are unnecessarily restrictive. The assumption of infinite gate-width in

Eqs. (77) and (78) implies that variation within the pulse of centroid position is not resolved. One could in principle find ''$x = 0$'', when in fact the head is at $+100$ μm, and the tail is at -100 μm. Where such intra-pulse resolution is required it is straightforward to extend our treatment to that case as well. Also, let us emphasize that Eq. (74) represents one choice as to the method of detection, and other choices are possible. For example, the modulus $|\tilde{V}_x \tilde{V}_\varphi^*|/|\tilde{V}_\varphi \tilde{V}_\varphi^*|$ also could be monitored to track drifts in ϕ. Our analysis indicates that this is not necessary. In addition, we point out that if one wishes to remove small nonlinearities in the transverse coordinate dependence, this could probably be accomplished by employing Eq. (74) for a first estimate of position in x and y, and then employing inferred coefficients B_n, and inferred cavity centroids to remove the residuals. Our analysis indicates that such a complex procedure is not necessary for 1 μm scale resolution.

A more subtle potential contributor to systematics arises from the effect of the cavity on the beam; let us show that this is a small effect. For the phase cavity, bunches will experience a retarding voltage on the order of $V \approx R_L I_b \equiv 2k_l Q_{eq}$. Using $R_L \approx 0.3$ MΩ, this corresponds to 30 kV/100 mA of beam current, a negligible induced energy spread. The position cavity of Sec. III also acts back on the beam, providing a transverse kick. The amplitude of the sinusoidal kick function may be expressed as $\Delta x' \approx e R_{\perp L} I_b x_b^2/mc\gamma$. Using $R_{\perp L} \approx 5.4 \times 10^3$ Ω/cm^2, and 45 GeV for the beam energy, this amounts to 1×10^{-12} rad/100 mA for a 100 μm beam offset. Actual deflection experienced by a bunch is reduced by an additional factor of order $\Omega \sigma_t \approx 10^{-2}$, arising from the 90° phase lag between the transverse and longitudinal kicks. This is a very small effect and can be neglected. It is not too surprising that kicks from the monitor are small, since the accelerator itself is made up of cells with similar characteristics.

V. DISCUSSION

In this work, we have characterized the coupling of cavity to a beam and an external waveguide. The multipole and parasitic mode effects are presently the primary limits to precision of cavities as resonant beamline pickups. They also limit future applications of miniature, planar accelerators. These effects dwarf the 10^{-13} W thermal noise in typical cavity bandwidths. We have set down a straightforward formulation of the problem, and illustrated it with an example of current interest for a fixed-target experiment. Two aspects of this work could bear improvement, and they concern the isolated resonance model for the cavity.

Historically, the formal treatment of a cavity in this way was first set down by Slater, with subsequent work by Kurokawa.[13] We have side stepped the full mathematical complexity of the problem by electing to consider isolated, narrowband cavity resonances. This is not the whole of the problem. First, as shown by Lin,[14] a cavity connected to a waveguide exhibits beam-induced fields with algebraic (non-exponential) decay. Their effect on the pickup has not been characterized here. In addition, frequencies above cutoff are also induced by the beam,[15] and the corresponding broadband impedance accounts for a significant fraction of parasitic energy loss by a beam in a cavity. Their coupling to the output structure is not well characterized, and further work could improve on this. Including such modes, and a few higher monopole modes still below cutoff, one may expect a parasitic mode voltage amplitude a factor of 2 or so higher than determined from the lowest monopole mode.

In the meantime, we have seen that in an asymmetric structure, the variation of $[R/Q]$ with transverse position has a fair variety to it, and is amenable to classification much as beamline magnets are. As in the case of beamline magnets, when precision is required, one is interested to know not only the dipole field on-axis, and the quadrupole gradient, but higher moments as well.

ACKNOWLEDGMENTS

[1] *The Two-Mile Accelerator*, edited by R. B. Neal (Benjamin, New York, 1968), pp. 500–516.

[2] T. Shintake, N. Akasaka, and S. C. Hartman, *Proceedings of the 1995 IEEE Particle Accelerator Conference* (IEEE, New York, 1995), pp. 2655–2657.

[3] R. Carr *et al.*, ''A Precision Measurement of the Weak Mixing Angle in Møller Scattering,'' SLAC-Proposal-E-158 (unpublished).

[4] M. Seidel, C. Adolphsen, R. Assmann, and D. H. Whittum, *Proceedings of the 1997 Particle Accelerator Conference* (IEEE, New York, 1998), pp. 2119–2121.

[5] M. Seidel, C. Adolphsen, K. L. F. Bane, R. M. Jones, N. M. Kroll, R. H. Miller, and D. H. Whittum, Nucl. Instrum. Methods Phys. Res. A **404**, 231 (1998).

[6] H. Henke, in *Advanced Accelerator Concepts*, edited by S. Chattopadhyay, J. McCullough, and P. Dahl, AIP Conf. Proc. 398 (AIP, New York, 1997), p. 485.

[7] P. J. Chou *et al.*, AIP Conf. Proc. **398**, 501 (1997).

[8] J. C. Slater, *Microwave Electronics* (Van Nostrand, New York, 1950).

[9] W. K. H. Panofsky and W. A. Wenzel, Rev. Sci. Instrum. **27**, 967 (1956).

[10] O. Altenmueller and P. Brunet, ''Some RF Characteristics of the Beam Phase Reference Cavity'' SLAC TN-64-51, Sept. 1964 (unpublished).

[11] W. Bruns, IEEE Trans. Magn. **32**, 1453 (1996).

[12] P. Brunet, J. Dobson, M. J. Lee, and C. B. Williams, ''Microwave Beam Position Monitors,'' SLAC TN 64-45, July, 1964 (unpublished).

[13] K. Kurokawa, IRE Trans. Microwave Theory Tech. **MTT-6**, 178 (1958).

[14] Xintian Lin, Ph.D. thesis, University of California at San Diego, 1995.

[15] A. W. Chao, *Physics of Collective Beam Instabilities in High Energy Accelerators* (Wiley, New York, 1993).